Dyes and Pigments 88 (2011) 262–273

Contents lists available at ScienceDirect

Dyes and Pigments

journal homepage: www.elsevier.com/locate/dyepig

Luminescent properties of some imidazole and oxazole based heterocycles: Synthesis, structure and substituent effects

Abiodun O. Eseola [a,d], Wen Li [b], Wen-Hua Sun [a,*], Min Zhang [a], Liwei Xiao [c], Joseph A.O. Woods [d]

[a] Key Laboratory of Engineering Plastics, Beijing National Laboratory for Molecular Science, Institute of Chemistry, Chinese Academy of Sciences, Beijing 100190, China
[b] Key Laboratory of Photochemical Conversion and Optoelectronic Materials, Technical Institute of Physics and Chemistry, Chinese Academy of Sciences, Beijing 100190, China
[c] Faculty of Chemistry and Material Science, Langfang Teachers College, Langfang 065000, China
[d] Department of Chemistry, Faculty of Science, University of Ibadan, Ibadan, Nigeria

ARTICLE INFO

Article history:
Received 26 January 2010
Received in revised form
10 July 2010
Accepted 12 July 2010
Available online 21 July 2010

Keywords:
Photoluminescence
Organic fluorescent photoswitch
Photo-aggregation
Solvent effects
Substituent effects
X-ray structures

ABSTRACT

A series of 2-R-6-(aryloxazol-/imidazol-2-yl)pyridine and 2,4-di-tert-butyl-6-(1H-phenanthro[9,10-d]imidazol-/oxazol-2-yl)phenol derivatives were synthesized and characterized using elemental and spectroscopic analyses as well as single-crystal X-ray diffraction analysis. The oxazole derivatives displayed higher photoluminescence efficiencies than their imidazole analogues. The 2-(phenanthro[9,10-d]oxazole/imidazol-2-yl)pyridine derivatives displayed quantum yields approaching unity in non-polar solvents but were quenched in polar solvents. The oxazole analogues produced reversible fluorescence photoswitching between 400 nm and 550 nm regions whilst the imidazole analogues underwent an irreversible photo-induced excimer formation in polar solvents. ^{1}H NMR was used to rationalize the proposed mode of intermolecular interactions between excimers of the 2-(phenanthro[9,10-d]imidazol-2-yl)pyridine derivatives.

1. Introduction

Research on organic luminescent materials has been keenly pursued because of their importance in technological applications related to signaling, fluorescent biosensory/chemosensory materials, molecular switches and organic light emitting diodes (OLEDs) [1–5]. Organic fluorophores, especially nitrogen-containing heterocyclic compounds, have attracted attention owing to their high emission efficiency [6–11]. However, as the basic structure of a fluorophore has to be modified, the investigation of substituent effects provides a route to optimizing potentially advantageous properties [12].

Though the naturally occurring jellyfish fluorescent proteins are the sole examples of biological molecules with photo-switching capability, synthetic molecules with controllable fluorescence switching in response to photo-irradiation are still being sought [11,13]. Although polymeric fluorophores offer durability as device components [14], small molecules are attractive as their structure–property relationships can be readily explored unlike polymeric materials [11]. Furthermore, polymeric fluorophores are usually fabricated by covalently grafting small size building blocks such as 2-(2-pyridyl)benzimidazole on to polymeric backbones [15,16]. Simple mixing of polymers with small M_r dyes has also been reported to give rugged fluorescent materials [17–19]. Rational tuning of desired characteristics is more achievable for small molecule fluorophores [20].

Molecules containing planar aromatic fragments such as pyrene, phenanthrene, anthracene, etc., are often found to exhibit robust photoluminescence properties that may be altered by presence or absence of intramolecular or intermolecular stacking interactions. Switching between free and assembled forms in solutions can be chemically [21] or solvent induced [22]. The phenomenon is also often manifested in significantly different emission spectral peaks positions and/or intensities obtained in solid and solution states of such fluorophores [22], however, there is rare report of synthetic fluorophores which undergoes solvent dependent photo-induced stacking in solution.

Numerous aryl-substituted imidazoles have been exploited for their emission properties in various research fields [23–32]. Most of this efforts have been largely spent on bidentate non-bridging imidazo[4,5-f][1,10]phenanthroline ligands and monodentate phenyl-substituted imidazoles. The systematic study of substituent effects on luminescent properties in this family of compounds is scarce and investigations on fluorescent imidazoles with receptor capabilities that involves the five-membered ring nitrogen as one of

* Corresponding author. Tel.: +86 10 62557955; fax: +86 10 62618239.
E-mail addresses: liwen@mail.ipc.ac.cn (W. Li), whsun@iccas.ac.cn (W.-H. Sun).

0143-7208/$ – see front matter © 2010 Elsevier Ltd. All rights reserved.
doi:10.1016/j.dyepig.2010.07.005

the donors have been largely restricted to 2-(2-pyridyl)benzimidazole [12,15]. To the best of our knowledge, photoluminescence research on 2-pyridyl-substituted oxazoles is not known. Recently, we accomplished preparation of a some new bidentate 2-(imidazol-2-yl/oxazol-2-yl)pyridine ligands capable of utilizing the imidazole base as one of the bidentate donors [33]. Considering the growing interests in organic fluorophores with receptor capabilities towards ions (metal or non-metal), this work presents a systematic comparison of the photoluminescent properties of twelve new fluorophores (**1**–**12**, Scheme 1a) based on imidazole/oxazole derivatives (Scheme 1b), from an experimental point of view. Syntheses of new compounds **3**, **4**, and **7**–**12** as well as X-ray structures of **8**, **9** and **11** are also herein reported. In efforts to rationalize nature of solute–solute interactions in solution, results of ^{1}H NMR studies of compounds **1**–**4** are also discussed.

2. Experimental

All starting materials were obtained commercially as reagent grade and used without further purification. Phenanthroline-5,6-dione was synthesized by literature procedure [34]. Compounds **1**, **2**, **5** and **6** were prepared according to our reported procedures [33]. Condensation reactions were carried out under nitrogen protection by use of standard Schlenk techniques. Organic compounds were purified on silica gel column to exclude impurities. Ethanol solvent was refluxed over CaH_2 and distilled prior to use. Elemental analyses were performed on a Flash EA 1112 microanalyzer. NMR spectra were recorded on a Bruker ARX-400 MHz instrument using TMS as internal standard. IR spectra were recorded on a Nicolet 6700 FT-IR spectrometer as KBr discs in the range of 4000–600 cm^{-1}. The steady-state fluorescence spectra were measured on F4500 – FL Fluorescence Spectrophotometer while fluorescence lifetimes were obtained by time-correlated single photon counting technique (Edinburgh Analytical Instruments F900 Fluorescence Spectrofluorimeter). Thin films were prepared on quartz slides with 1 cm width by spin coating. Fluorescence quantum yields (Φ_F) were calculated by comparative method using anthracene as standard [35,36].

$$\Phi_{F,x} = \Phi_{F,std}\frac{\int I_{F,x}(\nu)d\nu}{\int I_{F,\mathrm{std}}(\nu)d\nu}\left(\frac{1-10^{-A_{\mathrm{std}}}}{1-10^{-A_x}}\right)\left(\frac{n_x}{n_{\mathrm{std}}}\right)^2$$

($I_{F,x}(\nu)$ and $I_{F,\mathrm{std}}(\nu)$ are fluorescence intensities at wavelength ν for sample and standard respectively; A_x and A_{std} are absorbance at excitation wavelength for sample x and standard respectively; n_x and n_{std} are refractive indices of solvents employed for sample and standard respectively).

2.1. Preparation of imidazoles/oxazoles

2-(6-methylpyridin-2-yl)-1H-phenanthro[9,10-d]imidazole (**3**) and **2-(6-methylpyridin-2-yl)phenanthro[9,10-d]oxazole** (**4**): Phenanthrenequinone (1.00 g, 4.80 mmol) and ammonium acetate (7.40 g, 0.096 mol) were placed in a reaction flask, charged with nitrogen. Ethanol (15 cm^3), dichloromethane (15 cm^3), a catalytic amount of glacial acetic acid (0.5 cm^3) and 6-methyl-2-pyridinecarboxaldehyde (0.63 g, 0.480 mmol) were added and the ensuing mixture was refluxed for 3 h. After cooling, the reaction mixture was neutralized using concentrated aqueous ammonia and the volume was reduced under reduced pressure. The organic components were extracted using dichloromethane (50 cm^3, trice) and the combined organic extracts was concentrated and purified on silica gel column using dichloromethane/petroleum ether (1:4) to elute the oxazole product first and then ethyl acetate/petroleum ether (1:4) to elute the imidazole product. Portions containing the products were concentrated and addition of petroleum ether gave **3** (0.61 g, 41.0%) and **4** (0.49 g, 33.2%) as off-white and white micro-crystals respectively.

Compound **3**: Mp. 218–220 °C. Selected IR peaks (KBr disc, cm^{-1}): ν 3435s, 3072s, 1615w, 1595s, 1573s, 1462vs, 1450vs, 1235s, 796s, 752vs. ^{1}H NMR ($CDCl_3$, 400 MHz, TMS): δ 11.15 (br, s, 1H); 8.76 (d, J = 8.0 Hz, 2H); 8.71 (d, J = 8.4 Hz, 1H); 8.32 (d, J = 8.0 Hz, 1H); 8.15 (d, J = 8.0 Hz, 1H); 7.77 (dd, J = 8.0 Hz, 1H); 7.66 (m, 4H); 7.21 (d, J = 7.6 Hz, 1H); 2.68 (s, 3H). ^{13}C NMR ($CDCl_3$, 100 MHz, TMS): 158.06, 148.54, 147.76, 137.49, 128.57, 127.06, 125.45, 123.59, 122.48, 118.15, 24.31. Anal. Calc. for $C_{21}H_{15}N_3\cdot H_2O$: C, 77.04; H, 5.23; N, 12.84. Found: C, 76.95; H, 5.18; N, 12.79.

Compound **4**: Mp. 199–201 °C. Selected IR peaks (KBr disc, cm^{-1}): ν 3061s, 1616s, 1591s, 1569vs, 1459vs, 1429vs, 1233vs, 1080vs, 798vs, 761vs. ^{1}H NMR ($CDCl_3$, 400 MHz, TMS): δ 8.75 (m, 3H); 8.47 (d, J = 6.8 Hz, 1H); 8.28 (d, J = 8.0 Hz, 1H); 7.82 (dd, J = 7.6 Hz, 1H); 7.74 (m, 4H); 7.34 (d, J = 7.6 Hz, 1H); 2.79 (s, 3H). ^{13}C NMR ($CDCl_3$, 100 MHz, TMS): 160.96, 159.58, 145.72, 145.57, 137.22, 135.59, 129.77, 129.11, 127.48, 127.27, 126.82, 126.36, 126.18, 124.97, 123.71, 123.40, 123.29, 121.47, 121.03, 120.33, 24.77. Anal. Calc. for $C_{21}H_{14}N_2O\cdot H_2O$: C, 76.81; H, 4.91; N, 8.53. Found: C, 77.18; H, 4.72; N, 8.54.

2-(pyridin-2-yl)-1H-imidazo[4,5-f][1,10]phenanthroline (**7**) and **2-(pyridin-2-yl)oxazolo[5,4-f][1,10]phenanthroline** (**8**): A mixture of phenanthroline-5,6-dione (5.00 g, 0.024 mol), ammonium acetate (37 g, 0.480 mol), glacial acetic acid as catalyst (1.00 cm^3) and 2-pyridinecarboxaldehyde (2.86 cm^3, 0.030 mol)

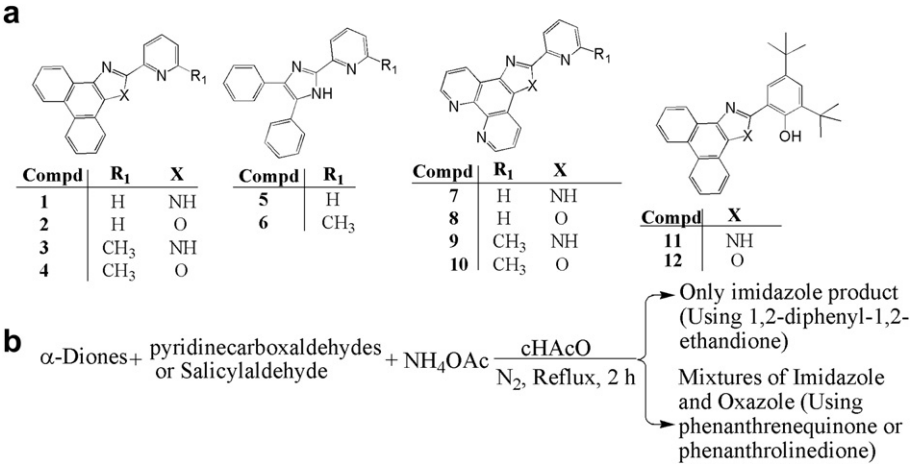

Scheme 1. (a) List of fluorophores studied in this work and (b) synthetic route to imidazole/oxazole compounds.

was treated according to procedure for **3** and **4** above except that chloroform was used in place of dichloromethane and the crude mixture was purified on silica gel column using ethanol/ethyl-acetate/petroleum ether (1:10:10) as eluent. The portions that contained pure products were concentrated and the precipitates were filtered, washed with small amount of ethanol and dried to afford isolated products of **7** (2.60 g, 36.4%) and **8** (0.67 g, 9.4%) as white powders. Single crystals of **8** suitable for X-ray analysis were grown by slow diffusion of n-hexane into its chloroform solution.

Compound **7**: Mp. >300 °C. Selected IR peaks (KBr disc, cm^{-1}): ν 3008m, 2944m, 1590s, 1562s, 1431vs, 1070m, 738vs. ^{1}H NMR (400 MHz, TMS, $CDCl_3$); δ 11.60 (br, s, 1H); 9.17 (d, J = 4.0 Hz, 2H); 9.05 (d, J = 8.0 Hz, 1H); 8.67 (d, J = 4.4 Hz, 1H); 8.52 (d, 7.6 Hz, 1H); 8.45 (d, J = 8.0 Hz, 1H); 7.92 (dd, J = 8 Hz, 1H); 7.74 (dd, J = 4.4, 8.0 Hz, 1H); 7.68 (dd, J = 4.4, 8.0 Hz, 1H); 7.39 (dd, J = 7.6 Hz, 1H). ^{13}C NMR (100 MHz, $CDCl_3$); 149.82, 149.17 148.84, 148.78, 148.05, 144.95, 144.78, 137.48, 137.35, 130.34, 128.85, 125.79, 124.40, 123.40, 122.84, 121.26, 118.95. Anal. Calc. for $C_{18}H_{11}N_5 \cdot ½H_2O$: C, 70.58; H, 3.95; N, 22.86%. Found: C, 70.96; H, 3.66; N, 22.93%.

Compound **8**: Mp. 269–271 °C. Selected IR peaks (KBr disc, cm^{-1}): ν 3053s, 2982m, 1584m, 1560m, 1456vs, 1446vs, 1059s, 741vs. ^{1}H NMR (400 MHz, TMS, $CDCl_3$); δ 9.26 (d, J = 3.8 Hz, 2H); 9.03 (dd, J = 1.7, 8.1 Hz, 1H); 8.91 (d, J = 4.5 Hz, 1H); 8.82 (dd, J = 1.7, 8.1 Hz, 1H); 8.47 (d, J = 7.9 Hz, 1H); 7.97 (dd, J = 7.9 Hz, 1H); 7.97 (m, 2H); 7.51 (dd, J = 4.8, 7.5 Hz, 1H). ^{13}C NMR (100 MHz, $CDCl_3$): 162.09, 150.47, 150.02, 149.82, 145.73, 145.19, 145.07, 144.04, 137.22, 134.77, 130.86, 129.01, 125.53, 123.64, 123.38, 123.25, 122.94, 117.97. Anal. calc. for $C_{18}H_{10}N_4O \cdot ½H_2O$: C, 70.35; H, 3.61; N, 18.23%. Found: C, 70.52; H, 3.65; 18.20%.

2-(6-methylpyridin-2-yl)-1H-imidazo[4,5-f][1,10]phenanthroline (**9**) and **2-(6-methylpyridin-2-yl)oxazolo[5,4-f][1,10]phenanthroline** (**10**): Phenanthroline-5,6-dione (3.00 g, 0.014 mol), ammonium acetate (22 g, 0.29 mol) and 6-methylpyridine-2-carboxaldehyde (2.1818 g, 1.25 equivalent) were reacted as described for **7** and **8** above to obtain **9** (1.10 g, 24.5%) and **10** (0.37 g, 8.2%) as light yellow and purple micro-crystals respectively. Single crystals of **9** suitable for X-ray analysis were grown by slow diffusion of n-hexane into its dichloromethane solution.

Compound **9**: Mp. >300 °C. Selected IR peaks (KBr disc, cm^{-1}): ν 3057s, 3016s, 1590m, 1562s, 1440s, 1068s, 739vs. ^{1}H NMR (400 MHz, TMS, $CDCl_3$); δ 11.60 (br, s, 1H); 9.17 (d, J = 4.1 Hz, 2H); 9.05 (d, J = 8.2 Hz, 1H); 8.49 (d, J = 7.7 Hz, 1H); 8.52 (d, 7.6 Hz, 1H); 8.30 (d, J = 8.0 Hz, 1H); 7.80 (dd, J = 7.7 Hz, 1H); 7.74 (dd, J = 4.4, 8.0 Hz, 1H); 7.68 (dd, J = 4.4, 8.0 Hz, 1H); 7.24 (d, partially overlapped with $CDCl_3$ residual peak, 1H); 2.66 (s, 3H). Anal. Calc. for $C_{19}H_{13}N_5$: C, 72.25; H, 4.31; N, 22.17%. Found: C, 72.47; H, 4.26; N, 22.05%.

Compound **10**; Mp. 266–268 °C. Selected IR peaks (KBr disc, cm^{-1}): ν 3016s, 1587s, 1558s, 1459vs, 1062s, 739vs. ^{1}H NMR (400 MHz, TMS, $CDCl_3$); δ 9.27 (dd, J = 2.0, 5.7 Hz, 2H); 9.05 (dd, J = 2.1, 10.8 Hz, 1H); 8.02 (dd, J = 2.1, 10.9 Hz, 1H); 8.28 (d, J = 10.3 Hz, 1H); 7.80 (m, 3H); 7.38 (d, J = 10.3 Hz, 1H); 2.79 (s, 3H). ^{13}C NMR (100 MHz, $CDCl_3$): 162.50, 159.85, 150.03, 149.75, 145.24, 145.09, 144.07, 137.40, 134.87, 131.20, 129.21, 125.54, 123.65, 123.40, 123.07, 120.62, 118.09, 24.79. Anal. calc. for $C_{19}H_{12}N_4O$: C, 73.07; H, 3.87; N, 17.94%. Found: C, 72.98; H, 3.85; N, 17.87%.

2,4-di-tert-butyl-6-(1H-phenanthro[9,10-d]imidazol-2-yl) phenol (**11**) and **2,4-di-tert-butyl-6-(phenanthro[9,10-d]oxazol-2-yl)phenol** (**12**): Phenanthrenequinone (2.00 g, 9.61 mmol), ammonium acetate (14.80 g, 0.192 mol) and 3,5-di-tert-butyl-2-hydroxybenzaldehyde (2.25 g, 9.61 mmol) were refluxed in glacial acetic acid (30 cm^3) for 3 h. After cooling, the reaction mixture was neutralized using concentrated aqueous ammonia and the crude product was filtered, dried and purified on silica gel column with dichloromethane/petroleum ether (1:10). The fractions containing pure products were combined, concentrated and allowed to stand to obtain isolated quantities of **11** as colourless crystals (0.22 g, 14.8%) and **12** as whitish micro-needles (0.52 g, 12.7%). Single crystals suitable for X-ray analysis were grown by slow evaporation of solvent from ethanol solution of the compound.

Compound **11**; Mp. >320 °C. Selected IR peaks (KBr disc, cm^{-1}): ν 3481m, 3348m, 3054m, 2957vs, 2906s, 2864s, 1615m, 1542m, 1509m, 747vs. ^{1}H NMR (400 MHz, TMS, $CDCl_3$); δ 13.40 (s, br, 1H); 10.01 (s, br, 1H); 8.73 (d, J = 8.0 Hz, 2H); 8.55 (br, 1H); 8.24 (br, 1H); 7.72 (m, 2H); 7.65 (br, 2H); 7.51 (br, 2H); 1.48 (s, 9H); 1.35 (s, 9H). Anal. Calc. for $C_{29}H_{30}N_2O$: C, 81.56; H, 7.20; N, 6.56. Found: C, 81.42; H, 7.11; N, 6.53.

Compound **12**; Mp. >300 °C. Selected IR peaks (KBr disc, cm^{-1}): ν 3077m, 3000m, 2962vs, 2907s, 2866s, 1618s, 1544s, 1255s, 749vs. ^{1}H NMR (400 MHz, TMS, $CDCl_3$); δ 12.03 (s, 1H); 8.76 (dd, J = 8.4 Hz, 2H); 8.55 (dd, J = 1.4 Hz, 8.0 Hz, 1H); 8.41 (d, J = 1.32 Hz, 8.2 Hz, 1H); 8.05 (d, J = 2.4 Hz, 1H); 7.73 (m, 4H); 7.54 (d, J = 2.4 Hz, 1H); 1.55 (s, 9H); 1.44 (s, 9H). Anal. Calc. for $C_{29}H_{29}NO_2$: C, 82.24; H, 6.90; N, 3.31. Found: C, 82.18; H, 6.94; N, 3.40.

2.2. X-ray measurements

X-ray single-crystal structure determination for compound **11** was carried out on Saturn724 using *CrystalClear* program (Rigaku Inc., 2008), while **8** and **9** were done on Rigaku R-AXIS Rapid IP diffractometer both employing graphite-monochromated Mo-Kα radiation and operated at −100 °C. Cell parameters were obtained by global refinement of the positions of all collected reflections.

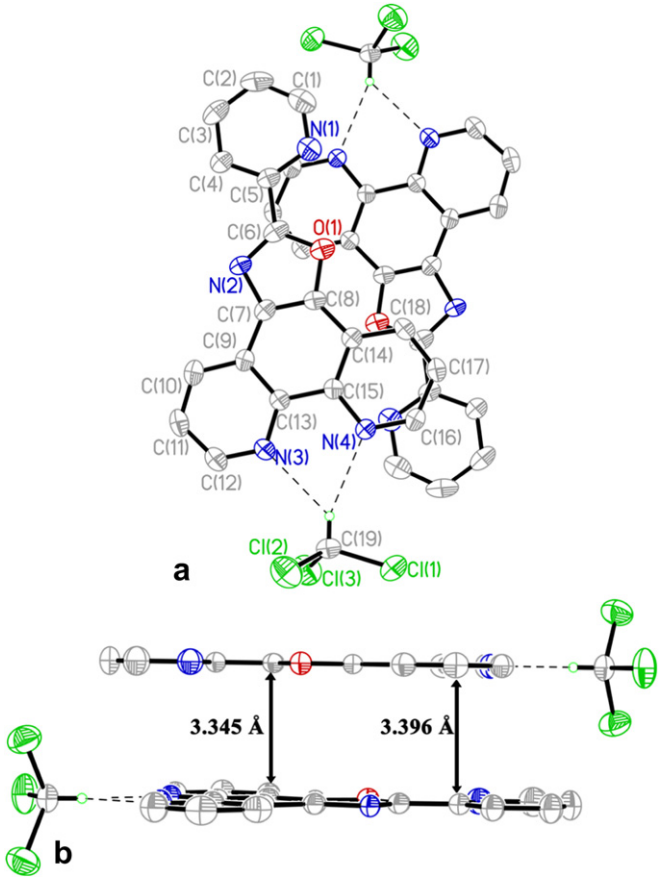

Fig. 1. Ortep plot of the molecular structure of 8·$CHCl_3$ showing (a) offset avoidance of stacking interaction and (b) planarity as well as separation between molecular planes. Some labels and hydrogen atoms have been omitted for clarity. Selected bond lengths (Å): O(1)–C(6) = 1.353(3); O(1)–C(8) = 1.372(3); N(2)–C(6) = 1.307(4); N(2)–C(7) = 1.387(3); N(1)–C(1) = 1.335(4); N(1)–C(5) = 1.346(4); C(4)–C(5) = 1.381(4).

Intensities were corrected for Lorentz and polarization effects and empirical absorptions. The structures were solved by direct methods and refined by full-matrix least-squares on F^2. All non-hydrogen atoms were refined anisotropically and all hydrogen atoms were placed in calculated positions. Structure solution and refinement were performed using the *SHELX-97* package [37].

3. Results and discussion

3.1. Synthesis of organic compounds

The compounds were obtained by condensation of α-diketones with the appropriate aryl aldehydes (pyridinecarboxaldehydes or 3,5-di-tert-butyl-2-hydroxybenzaldehyde) under reflux and in the presence of excess ammonium acetate (Scheme 1b). Unlike for 1,2-diphenyl-1,2-ethanedione, which forms only the imidazole condensation product, phenanthrenequinone or phenanthroline-5,6-dione yielded both imidazole and oxazole products competitively. The rigidity and co-planarity of the carbonyl groups in the fused-ring starting materials enabled close proximity of heteroatoms towards competitive cyclization of N^N diimine and N^**O** keto-imime intermediates [33]. The oxazole products could be differentiated from the imidazole products on the basis of ^{1}H NMR, ^{13}C NMR, melting point and elemental analysis. The imidazole active proton, which was absent in ^{1}H NMR spectra of the oxazole analogues, could be seen at around δ 11.5 ppm for the pyridyl molecules and at δ 13.4 ppm for the phenolic ligand **11**. Due to stronger deshielding, the ^{13}C NMR spectra of the oxazoles all gave the most downfield δ peaks within 163.0–160.0 ppm while the imidazoles gave the corresponding peak between 158.0 and 148.0 ppm. The peak is assigned to the 2-imidazole carbon between the two heteroatoms of the oxazole (e.g. C(6), Fig. 1a) or imidazole rings (e.g. C(6), Fig. 2a). Moreover, there were more separations of the ^{13}C NMR peaks in the spectra of oxazoles unlike the observed clustering of peaks obtained for the imidazoles. Electronically, the imidazoles are expected to have higher charge symmetry and equivalent carbon atoms. The oxazoles generally exhibited significantly lower melting points relative to the imidazoles. Compounds **1**, **2**, **5** and **6** were obtained according to recently published method [33].

3.2. X-ray structures

Molecular structures of **8**, **9** and **11** were confirmed by X-ray experiments. Compound **8** crystallized in orthorhombic Pnma space group while compounds **9** and **11** crystallized in triclinic P-1 space group all with four molecules in each unit cell. Crystallographic data and refinement details are tabulated in Table 1.

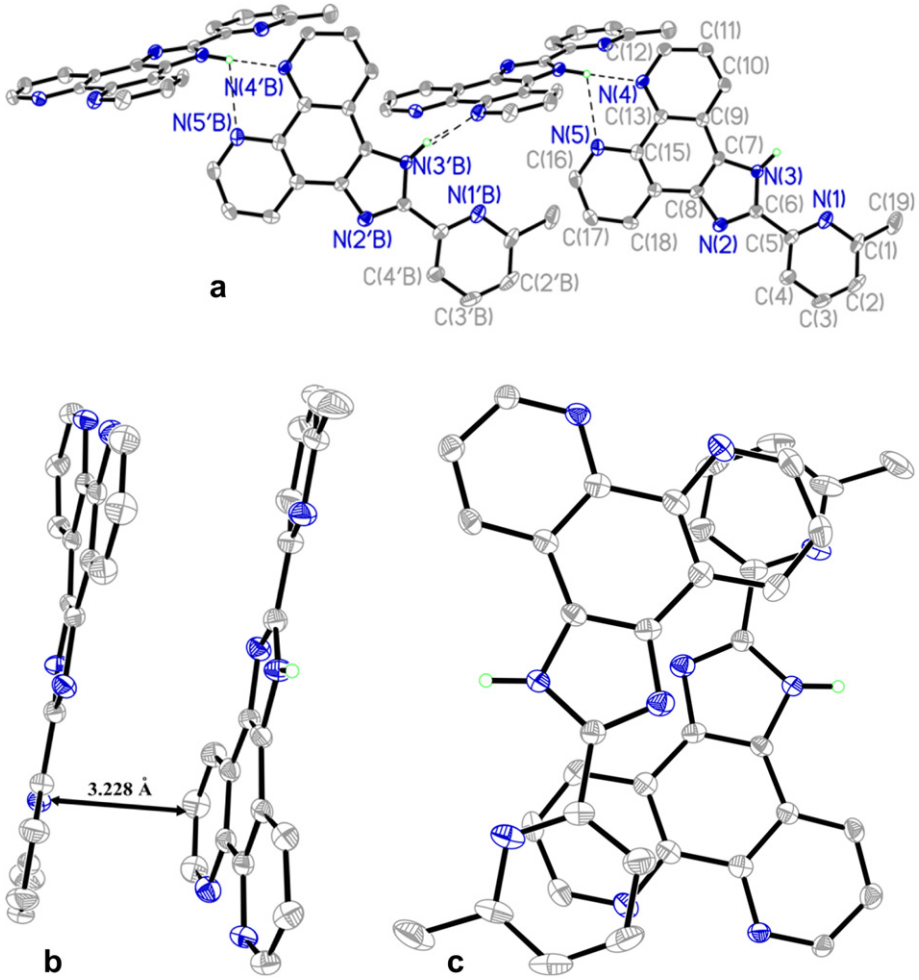

Fig. 2. Ortep plot of the molecular structure of 9 showing (a) 1-Dimentional hydrogen bonding chain, (b) stacking separation distance and lower co-planarity between pyridyl ring and the rest of the molecule, and (c) partial face-to-face stacking mode. Some hydrogen atoms and labels have been omitted for clarity. Selected bond lengths (Å): N(1)–C(1) = 1.340 (4); N(1)–C(5) = 1.340(4); N(2)–C(6) = 1.331(4); N(2)–C(8) = 1.369(4); N(3)–C(6) = 1.361(4); N(3)–C(7) = 1.371(4); N(3)–H(3N) = 1.0285; C(4)–C(5) = 1.384(5); N(2′)–C (6′) = 1.317(4); N(2′)–C(8′) = 1.375(4); N(1′)–C(5′) = 1.337(5); N(1′)–C(1′) = 1.339(4); N(3′)–C(6′) = 1.364(4); N(3′)–C(7′) = 1.380(4); C(4′)–C(5′) = 1.379(5).

The molecular structure of compound **8** is shown in Fig. 1 with the selected bond lengths around heteroatoms of the pyridyl and oxazolyl rings. The discrete adduct of chloroform was observed and completely devoid of networking or stacking interactions. The observation is considered to result from absence of active protons as in imidazoles, which usually exhibits one dimension (1-D) networks [38]. Noteworthy also is the co-planarity (0°) between the pyridyl plane {O(1)–N(2)–C(6)–C(7)–C(8)} and the plane occupied by the oxazole ring atoms {N(1)–C(1)–C(2)–C(3)–C(4)–C(5)} (Fig. 1a and b). This may imply an optimum π-conjugation between the pyridyl ring aromatic system and the rest of the molecule. The complete offset interaction in the structure of compound **8**, which is totally devoid of stacking, is worthy of note (Fig. 1a and b). Furthermore, the separation between the plane of one molecule and another (3.396–3.345 Å) is larger than observed value for the closely related imidazole analogue **9**. It could be conclude that the oxazolyl derivatives possess inherently weaker intermolecular interaction tendencies.

Imidazole compound **9** maintains a 1-D chain involving hydrogen bonds between imidazole proton of one molecule and the phenanthrolineyl nitrogen atoms of the next molecule (Fig. 2a). A twist as large as 10.92° between the pyridyl ring {C(5)–C(4)–C(3)–C(2)–C(1)–N(1)} and the phenanthrolineyl moiety {N4–C12–C11–C10–C9–C13–N5–C16–C17–C18–C14–C15} was observed (Fig. 2a), which has significance on extent of overlap that is possible between the pyridyl π-system and imidazo-phenanthroline bulk. As shown in Fig. 2b and c, it could also be observed that a significantly shorter π-stacking distance exists between the pyridyl ring of one molecule {N(1)–C(3)–C(2)–C(1)–C(4)–C(5)} and one of the phenanthrolineyl rings of an adjacent partner {N(5)–C(12)–C(11)–C(10)–C(13)–C(9)} with a separation of 3.228 Å.

Though attempts to obtain suitable single crystals for the phenanthrene-substituted compounds **1**–**4** yielded twined crystals for the imidazoles (**1** and **3**) and tiny needles for the oxazoles (**2** and **4**), it was anticipated that the phenol compound **11** would give a clue about intermolecular interactions for the phenanthreneyl systems. X-ray analysis for compound **11** revealed two crystallographically independent molecules that consist of one flat molecule with disordered *t*Bu and oxo atoms and another bent, but non-disordered molecule (Fig. 3a). The angle of bending over between the phenol plane {C(6)–C(4)–C(2)–C(3)–C(5)–C(1)} and the phenanthreneyl fragment {C(10)–C(8)–C(9)–C(16)–C(17)–C(15)} in the tilted molecule is as large as 14.66°. Moreover, the crystal structure revealed that the disordered, flat molecule exists in Zwitterionic form in which the phenolic proton is bonded to the imidazole ring to yield oxo anion on phenol ring and imidazolium cation. The phenolic proton of the second molecule is intact (Fig. 3a and c). In fact, the imidazole protons were quite obvious on the difference map and were picked before fixing all protons in calculated positions in the course of structure refinement for compound **11**. The notable difference (0.034 Å) in the imidazole ring bond lengths N(3)–C(7) (1.334(2) Å) and N(4)–C(7) (1.368(3) Å) observed for the bent molecule in contrast to the insignificant difference (0.001 Å) for the corresponding bonds of the imidazolium ring of the flat molecule {N(2)–C(36) = 1.344(3) Å; N(1)–C(36) = 1.345(3) Å} supports existence of Zwitterionic structure of the flat molecule. Compound **11** also revealed strong π–π interactions (Fig. 3b) between the phenanthrene rings (3.321 Å), which held the molecules into repeating tetrameric packs (Fig. 3c).

The observed face-to-face interactions, which are due to the rigid planar nature of the compounds **8**, **9** and **11**, are considered to suggest poorer intermolecular interaction tendencies in oxazoles and stronger interactions for the imidazoles. Although the role of solvent of crystallization and crystal packing forces may be significant, the stacking distances suggests that a more stable face-to-face interaction would be expected for imidazole frameworks than for the oxazoles.

Table 1
Crystallographic data and refinement details for **8**, **9** and **11**.

Parameters	**8**.$CHCl_3$	**9**	**11**
Formula	$C_{19}H_{11}C_{l3}N_4O$	$C_{19}H_{13}N_5$	$C_{29}H_{30}N_2O$
Fw	417.67	311.34	422.55
Temperature (K)	173(2)	173(2)	173(2)
Wavelength (Å)	0.71073	0.71073	0.710747
Crystal system	Orthorombic	Triclinic	Triclinic
space group	Pnma	P-1	P-1
a (Å)	9.814(2)	10.008(2)	10.109(2)
b (Å)	6.6845(13)	12.402(3)	13.670(3)
c (Å)	27.146(5)	12.504(3)	17.355(3)
α (deg)	90.00(0)	88.88(3)	101.33(3)
β (deg)	90.00(0)	78.17(3)	101.23(3)
γ (deg)	90.00(0)	75.05(3)	96.15(4)
Volume ($Å^3$)	1780.8(6)	1466.7(5)	2279.9(8)
Z	4	4	4
Calculated density (g cm^{-3})	1.558	1.410	1.231
μ (mm^{-1})	0.532	0.089	0.074
F(000)	848	648	904
Crystal size (mm)	0.78 × 0.71 × 0.38	0.66 × 0.34 × 0.18	0.34 × 0.30 × 0.26
θ range (deg)	1.50–27.47	2.37–25.00	1.54–27.49
Limiting indicates	$-12 \le h \le 12$	$-11 \le h \le 11$	$-13 \le h \le 13$
	$-8 \le k \le 8$	$-14 \le k \le 14$	$-17 \le k \le 17$
	$-35 \le l \le 35$	$-14 \le l \le 14$	$-22 \le l \le 22$
No. of rflns collected	3935	9390	28039
No. of unique rflns	2221	5143	10392
R(int)	0.0168	0.0483	0.0396
Completeness (%) to θ (°)	99.9, θ = 27.47	99.7, θ = 25.00	99.4, θ = 27.49
No. of parameters	161	445	652
Goodness-of-fit on F^2	1.130	1.317	1.144
Final R indices (I > 2sigma(I))	$R1$ = 0.0431	$R1$ = 0.0938	$R1$ = 0.0756
	wR2 = 0.1167	wR2 = 0.1550	wR2 = 0.1916
R indices (all data)	$R1$ = 0.0572	$R1$ = 0.1266	$R1$ = 0.0875
	wR2 = 0.1343	wR2 = 0.1657	wR2 = 0.2001
Largest diff. peak and hole (e $Å^{-3}$)	0.541, −0.445	0.272, −0.272	0.408, −0.410

3.3. *Absorption properties of compounds **1**–**12***

The absorption spectra of compounds **1**–**4** in cyclohexane and dichloromethane as well as those of compounds **5**–**12** in EtOH are presented in Fig. 4a–d. Comparing the respective absorption bands of the phenanthreneyl derivatives **1**–**4**, it is noteworthy that the oxazoles **2** and **4** absorbed at relatively blue shifted wavelengths compared to the imidazoles **1** and **3** (Fig. 4a). This suggests more electron delocalization in **1** and **3** than for **2** and **4**. Lower electronic conjugation by the oxazole ring should be expected on account of non-bonding electronic orbital orientation and greater electronegativity of the oxo atom. However, the band shapes are generally the same for the oxazoles as for the imidazoles. The rest of the imidazole/oxazole pairs generally maintained the same absorption maximums for the oxazoles as for the corresponding imidazoles (**7** versus **8**, **9** versus **10** and **11** versus **12**; Table 2). Furthermore, the extended conjugation offered by presence of the phenanthrene group is reflected by longer absorption wavelength bands in the region 359–367 nm observed for **1**–**4**, **11** and **12**. Shorter absorption wavelengths in the range of 323–331 nm were recorded for the diphenyl-substituted (**5** and **6**) and phenanthrolineyl-substituted (**7**–**10**) derivatives, and indicate lower extent of π conjugation. The shorter wavelength absorption bands for the phenanthrolineyl analogues **7**–**10** could be attributed to perturbation of π–electron system due to difference of nitrogen as heteroatom.

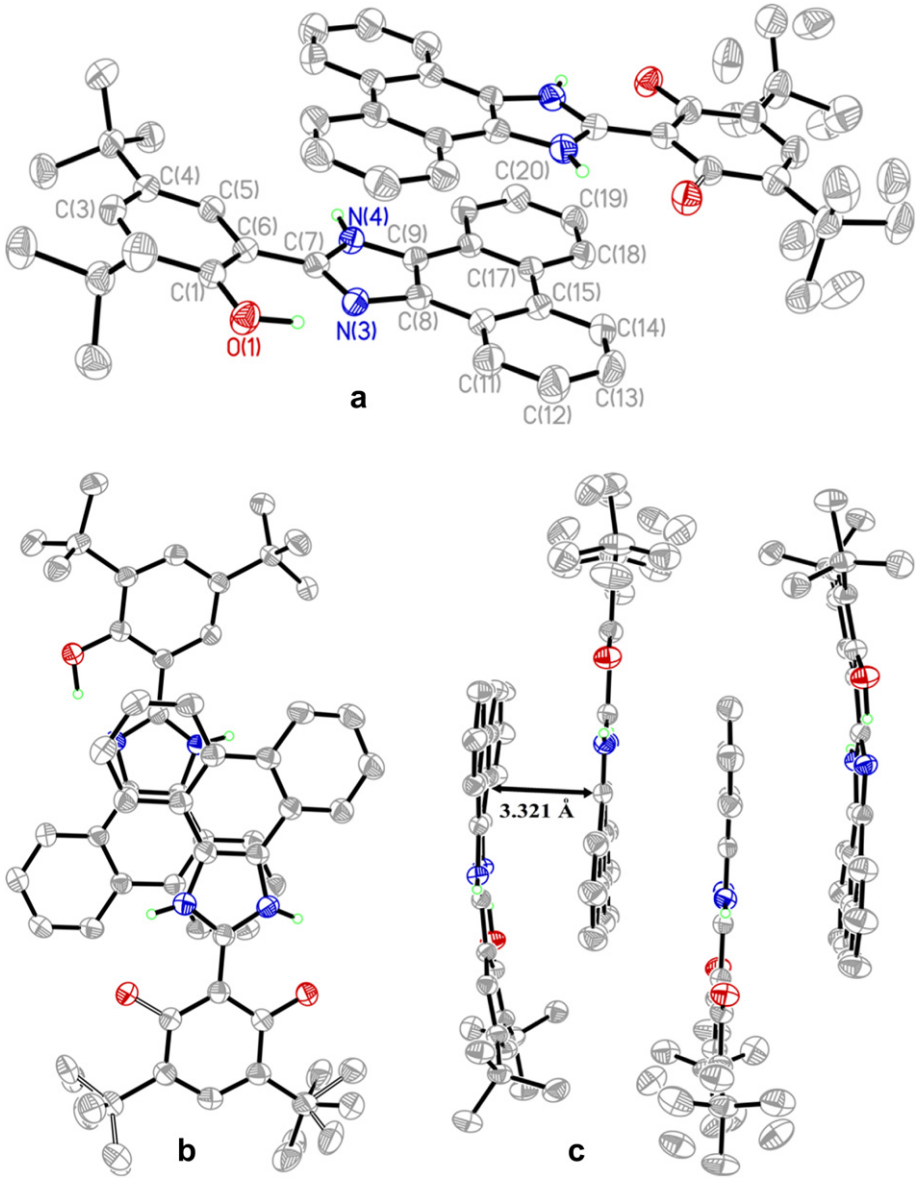

Fig. 3. Ortep plot of **11** showing (a) two crystallographically independent molecules, (b) their mode of π–π stacking interaction, and (c) tetrameric packing. Some labels and hydrogen atoms have been omitted for clarity. Selected bond lengths (Å): O(1)–C(1) = 1.355(2); N(3)–C(7) = 1.334(2); N(3)–C(8) = 1.383(3); N(4)–C(7) = 1.368(3); N(4)–C(9) = 1.376(2); N(4)–H(4N) = 0.8904; N(1)–C(37) = 1.377(3); N(1)–H(1N) = 0.8800; N(2)–C(36) = 1.344(3); N(2)–C(38) = 1.378(3); N(2)–H(2N) = 0.8800; C(34)–O(2) = 1.349(4); C(30)–O(2′) = 1.333(3); O(2)–H(30′) = 0.3936; O(2′)–H(30) = 0.3757.

Methyl substitution did not yield any obvious difference in absorption properties of substituted derivatives compared to unsubstituted derivatives (e.g. **5** and **6**; Table 2). On the basis of band shapes and wavelengths, it could be concluded that the spectroscopic properties of the series are largely dependent on substituent attached to the 4,5-positions of the imidazole ring. On exposure to UV radiation (355 nm), compounds **1** and **3** exhibit new broad absorption peaks around 430 nm (Fig. 4b). This absorbing species have been attributed to π–π stacked aggregate formation that is photo-induced. Further experiments were conceived and executed to explore the nature of excimer formed.

3.4. Photoluminescence properties of compounds 1–12

All emission scans were carried out at room temperature using same concentration (5×10^{-5} mol dm^{-3}). The photoluminescence spectra of all compounds were obtained in cyclohexane and ethanol. Observed photoluminescence parameters are summarized in Table 2. It could be noticed that compounds **1**–**10** gave the primary excited state emissions in the blue region of the visible spectrum (368–416 nm) while compounds **11** and **12** produced large Stokes shifted secondary emissions in the green region (470–508 nm) as a result of excited state intramolecular proton–electron transfer (ESIPT) process (Table 2) [38]. According to X-ray diffraction pattern, existence of Zwitterions in solid state of **11** (Fig. 3a) suggests the ease for achieving photo-induced ESIPT emissions in **11**–**12**. Emission lifetimes in the various solvents confirm fluorescent nature of the emissions rather than phosphorescence (Table 2).

One notable observation in the photoluminescence data for the pyridyl derivatives **1**–**10** (Table 2) is the strong similarities in fluorescent parameters between 6-methyl-substituted compounds and their corresponding unsubstituted analogues in terms of fluorescence quantum yield Φ_F, photoluminescence lifetime τ and energy separation between ground state S_o and the first excited

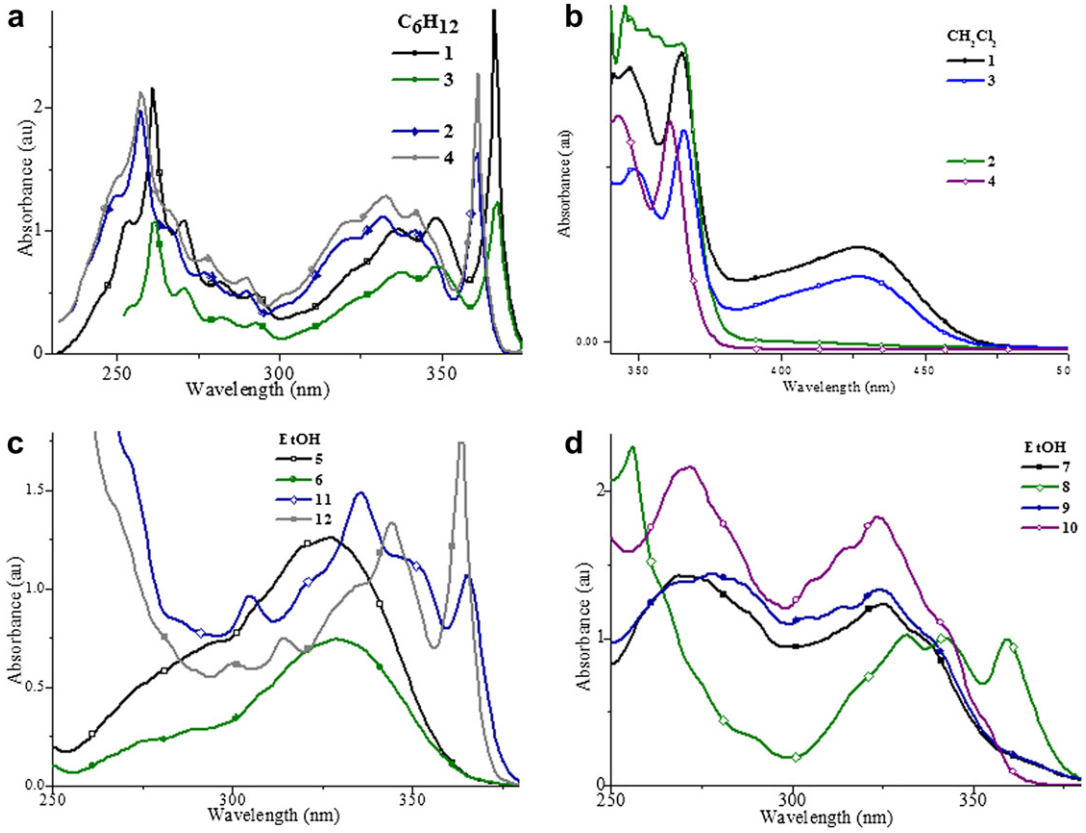

Fig. 4. Absorption spectra of (a) **1**–**4** in cyclohexane showing blue shift of the oxazoles (**2** and **4**) relative to the imidazoles (**1** and **2**); (b) 1–4 in dichloromethane showing excimer absorption for compounds **1** and **3** after exposure to UV; (c) **5**, **6**, **11** and **12** in EtOH; (d) **7**, **8**, **9** and **10** in EtOH. (For interpretation of the references to colour in this figure legend, the reader is referred to the web version of this article).

state S_1 (e.g. for imidazo-pyridines, Fig. 5a: **1** versus **3**, **5** versus **6**, **7** versus **9**; e.g. for oxazo-pyridines, Fig. 5b: **2** versus **4**, **8** versus **10**). Therefore, methyl substituent in the ortho-position to pyridyl nitrogen neither produced significant effects on ground and excited state energies nor on excited state photo-relaxation processes for this family of molecules in solution. In the various solvents, oxazole analogues were observed to exhibit stronger photoluminescence efficiencies in comparison with their respective imidazole derivatives (Table 2: **1** versus **2**, **3** versus **4**, **7** versus **8**, **9** versus **10**). It could be reasoned that the presence of active imidazolyl proton would enhance non-radiative relaxation processes via solvent–solute or solute–solute interactions. This view is supported by the extensive intermolecular interactions in the solid state structures of compounds **9** and **11** (Figs. 2 and 3), which is absent in the oxazole compound **8** (Fig. 1). An additional probable reason is the better co-planarity in the oxazole compounds than the imidazole compound as suggested by crystal structure of compound **8**. This factor is favorable for enhancement of fluorescence efficiency through better electronic overlap of the aromatic system of the pyridyl ring and the oxazo-phenanthreneyl moieties. Furthermore, dramatic reduction of quantum yields in going from non-polar cyclohexane systems to the more polar ethanol solutions is in agreement with the proposed role of intermolecular interactions towards reducing fluorescence quantum yields. According to Table 2, this solvent effect is more pronounced for imidazoles (e.g. **1**, $\Phi_{F,\ \text{Cyclohexane}} = 0.69$ versus $\Phi_{F,\ \text{Ethanol}} = 0.02$; **3**, $\Phi_{F,\ \text{cyclohexane}} = 0.97$, $\Phi_{F,\ \text{Ethanol}} = 0.02$) than for the oxazoles (e.g. **2**, $\Phi_{F,\ \text{Cyclohexane}} = 0.83$ versus $\Phi_{F,\ \text{Ethanol}} = 0.16$; **4**, $\Phi_{F,\ \text{Cyclohexane}} = 0.95$ versus $\Phi_{F,\ \text{Ethanol}} = 0.16$). For the pyridyl molecules **1**–**10** in cyclohexane, substituent effects on photoluminescence efficiencies at the 4,5-position of the five-membered ring gave a general order of phenanthreneyl > 4,5-diphenyl > phenanthrolineyl (Table 2), which it is in accordance with capacity of their molecular structures to delocalized π–electrons. However, the quantum yield values in ethanol maintained quite lower and similar values.

The ESIPT emissions of compounds **11** and **12** appeared to exhibit opposite trends of the above observations. Furthermore, the relatively lower quantum yields observed for compounds **11** and **12** could be ascribed to inherent vibrational quenching due to the two *t*Bu substituents (Fig. 5b red trace).

3.5. Photo-induced fluorescence switching of compounds *1*–*4*

It was discovered that compounds **1**–**4** possessed some interesting properties worthy of further examination. Compounds **1** and **3** were observed to undergo photo-induced excimer formation with broad absorption band around 425 nm (Fig. 4b) and corresponding excimer emission around 550 nm in ethanol (Table 2) or 500 nm in dichloromethane (Table 3, Fig. 6a). Such excimer formation was not observed in the non-polar cyclohexane. Also an interesting fact is that, unlike for any other compound in the studied series, compound **3** displayed a very brilliant solid film photoluminescence in the green region of the visible spectrum at room temperature (Fig. 7a). Besides electronic effects, there is probably an interesting steric effect of the methyl group on molecular arrangements in solid state, and is probably an evidence of different solid state molecular arrangements in **3** compared to **1**.

Though the exact mechanism for forming the new solution species via excited states is still not clear, experimental findings suggests that, depending on solvent properties, the molecules

Table 2
Absorption and photoluminescence data (**1**–**12**) in cyclohexane and ethanol.

	Compounds	$\lambda_{abs\text{-}max}$ (nm)	$\lambda_{Ex\text{-}max}$ (nm)	$\lambda_{Em\text{-}max}$ (nm)[d]	Stokes shift (nm)[d]	τ(ns)[d]	Φ_F[e]	$k_r \times 10^8 (S^{-1})$	$k_{nr} \times 10^8 (S^{-1})$
C_6H_{12}	**1**	348, 366	360	389	29	2.0	0.69	3.450	1.550
EtOH		346, 363	357	394 [**555**]	37 [**198**]	2.1 [**4.4**]	0.02	0.095 [**0.045**]	4.667 [**2.227**]
C_6H_{12}	**2**	332, 361	355	383	28	2.4	0.83	3.458	0.708
EtOH		342, 359	366	406	40	2.3	0.16	0.696	3.652
C_6H_{12}	**3**	348, 367	360	390	30	2.0	0.97	4.850	0.150
EtOH		346, 363	357	393 [**550**]	36 [**193**]	2.0 [**4.6**]	0.02	0.100 [**0.043**]	4.900 [**2.130**]
Film				**518**					
C_6H_{12}	**4**	333, 361	352	383	31	–[b]	0.95	–	–
EtOH		342, 360	364	404	40	2.2	0.16	0.727	3.818
C_6H_{12}	**5**	331	350	386	36	2.4	0.26	1.083	**3.083**
EtOH		327	348	397	49	1.6	0.01	0.063	**6.188**
C_6H_{12}	**6**	331	342	385	43	0.7	0.35	5.000	**9.286**
EtOH		329	342	394	52	1.4	0.01	0.071	**7.071**
C_6H_{12}	**7**	–[a]	368	389	21	–[c]	–[c]	–	–
EtOH		272, 325	348	412	64	4.9	0.03	0.061	1.980
C_6H_{12}	**8**	280, 328	328	375	47	1.3	0.18	1.385	6.308
EtOH		272, 323	347	382	35	3.5	0.03	0.086	2.771
C_6H_{12}	**9**	–[a]	337	368	31	–[c]	–[c]	–	–
EtOH		278, 324	350	416	66	5.0	0.03	0.060	1.940
C_6H_{12}	**10**	272, 328	329	376	47	1.4	0.16	1.143	6.000
EtOH		272, 324	352	385	33	3.7	0.03	0.081	2.622
Film				443					
C_6H_{12}	**11**	340, 366	360	492	132	3.5	0.23	0.657	2.200
EtOH		336, 365	370	470	100	2.8	0.06	0.214	3.357
Film				481					
C_6H_{12}	**12**	345, 365	358	508	150	–[c]	–[c]	–	–
EtOH		344, 363	357	508	151	4.0	<0.01	>0.025	>2.475
Film				494					

[a] Low solubility.
[b] Value was in same range with response factor.
[c] Signal too weak due to low solubility.
[d] τ represents fluorescence emission lifetimes and values in square bracket represent photo-induced excimer emission data.
[e] Φ_F is fluorescence quantum yield for primary emissions.

undergo some sort of intermolecular adduct formation/aggregation, which is of a rather high stability for compounds **1** and **3**, but reversible in the case of compounds **2** and **4**. This proposed aggregate formation is supported by emission wavelengths occurring in the red-shifted region for photo-generated species in solutions as for solid film of compound **3** (Table 2). Attempts to obtain suitable single crystals for compounds **1** and **3** only yielded twined crystals. This is thought to result from incorporation of already assembled aggregate units along with single molecules into growing crystal lattices. Though the "offset face-to-face" stacking

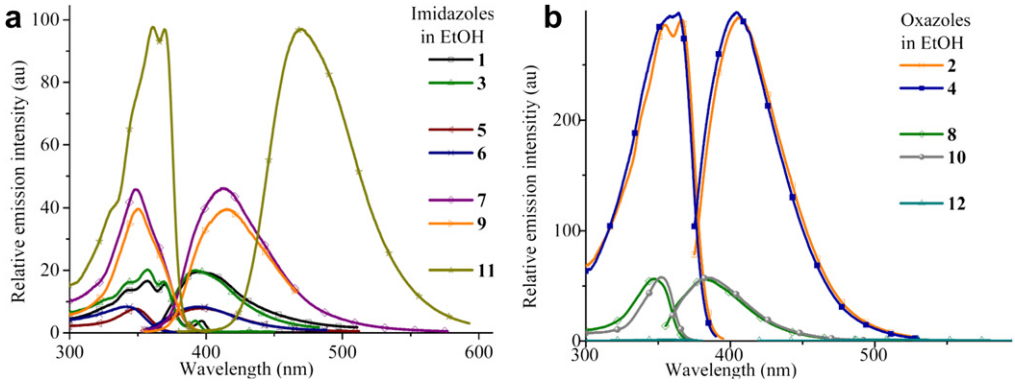

Fig. 5. Excitation and photoluminescence spectra for (a) imidazole compounds **1**, **3**, **5**, **6**, **7**, **9** and **11**, and (b) oxazole compounds **2**, **4**, **8**, **10** and **12** in ethanol. Emission scans were excited at excitation maxima.

Table 3
Photoluminescence data for compounds **1**–**4** in CH_2Cl_2 and CH_3CN.

	Compounds	λ_{Ex-max} (nm)	λ_{Em-max} (nm)[a]	Stokes shift (nm)[a]	τ (ns)[b]
CH_2Cl_2	**1**	367	401[**503**]	34 [**136**]	6.1
CH_3CN		ND[c]	395, **775**	ND[c]	1.9
CH_2Cl_2	**2**	369	403	34	2.9
CH_3CN		ND	405, **785**	ND	2.1
CH_2Cl_2	**3**	364	395 [**500**]	31 [**136**]	
CH_3CN		ND	395, **775**	ND	2.2
CH_2Cl_2	**4**	353	399	46	
CH_3CN		ND	405, **790**	ND	2.1

[a] Values in square bracket represent photo-induced excimer emission data.
[b] Primary emission lifetime; same values were obtained for both visible and near-infrared emissions.
[c] ND = Not determined.

patterns observed in the structures of compounds **9** and **11** (Figs. 2c and 3c) affords a clue about possible intermolecular arrangements leading to the species formed after photo-irradiation, possibility of solvent–solute adduct aggregation can not be dismissed.

Except for the cases of cyclohexane solutions of compounds **1**–**4**, it was found that the rate of non-radiative events k_{nr} effectively outweighed radiative rates k_r in depopulating the excited states for solutions of compounds **1**–**12** at room temperature. The derived radiative/non-radiative lifetime data (Table 2) suggest the importance of polar–polar interactions in depopulating the excited state since the more polar ethanol solutions generally yielded larger non-radiative rates. The exceptions found in non-polar solvent for the phenanthreneyl ligands **1**–**4** could be attributed to the more stable conjugation in the phenanthreneyl ligands, which is probably as a result of lesser number of heteroatoms resulting in lesser probabilities of polar interactions between the fluorophores and neighbouring molecules. Although compounds **5** and **6** were anticipated to give similar emission characteristics as for compounds **1** and **3** in cyclohexane on account of same heteroatom substitution, compounds **5** and **6** should possess additional inherent thermal deactivation due to vibrations of the pendant phenyl substituents on the 4- and 5-positions of the imidazole ring. This conclusion is supported by the obviously larger non-radiative rates in both non-polar and polar solvents (Table 2). The methyl substituent did not have any notable effects on k_r and k_{nr} values. The longer lifetime of emissions from photo-induced excimer species coupled with their k_r and k_{nr} values that are lower than for the corresponding k_r and k_{nr} values for the emissions of free molecule also suggests formation of a more rigid/larger photo-aggregation species, which may involve stacking.

Assignment of longer wavelength emissions to stacking of planar moieties is known for some pyreneyl [21,22] and xanthone compounds [39]. However, to the best of our knowledge, such photo-induced process as observed for **1** and **3** is not known. Another interesting feature of compounds **2** and **4** is the photo-switching of emission band between the 400 nm and 550 nm regions of the visible spectrum. It is believed that the new, short-lived emission bands that appear at red-shifted wavelengths resulted from photo-induced excimer species. Fluorescence lifetimes for compounds **1**–**4** as further explored in acetonitrile were generally of the order of nanoseconds (ns). The short-lived species for compounds **1** and **3** quickly reverts to the initial species after the laser source is turned off (Fig. 6b). This "on–off" photo-switching of emission may be of potential application in molecular signaling.

The results for further measurements in dichloromethane and acetonitrile, which were recorded to further investigate the characteristics of the new fluorophores formed after photo-excitation of compounds **1**–**4**, are presented in Table 3. Generally,

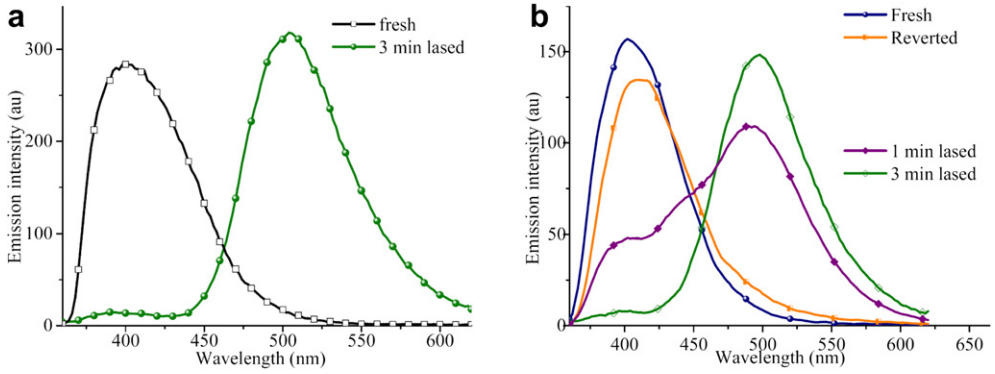

Fig. 6. 355 nm Laser flash-photolysis experiments in dichloromethane showing (a) irreversible photo-aggregation of compound **1** and (b) photo-switching behaviour of compound **2**.

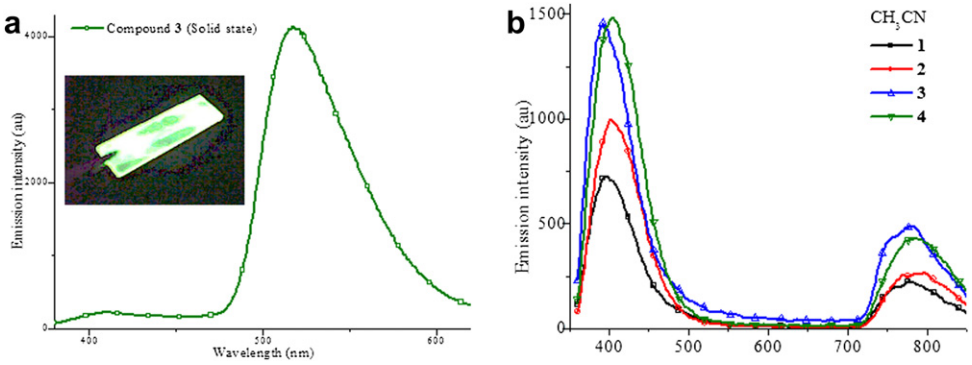

Fig. 7. Photoluminescence spectra of (a) compound **3** as solid thin film and (b) compounds **1**–**4** in acetonitrile showing the strong near-infrared emissions.

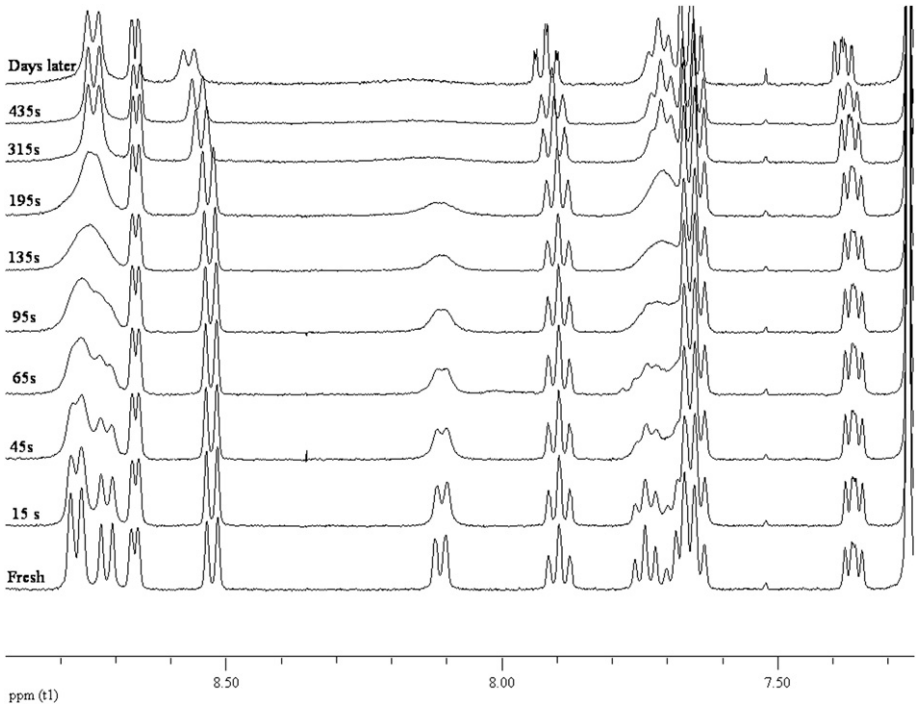

Fig. 8. Vertical stack of ^{1}H NMR of **1** in $CDCl_3$ at increasing exposure to UV radiation (300 nm).

trends in these data are comparable to those observed in ethanol. Furthermore, near-infrared emission bands, which were quite weak in ethanol, cyclohexane and dichloromethane, were considerably stronger in the acetonitrile spectra (Fig. 7b). Therefore, it is concluded that there is a strong dependence of photoluminescence characteristics on nature of condensed media for the investigated molecules.

3.6. ^{1}H NMR studies

It is anticipated that the affected protons of compounds **1**–**4** in the photo-induced intermolecular interactions should be broadened and/or shifted while the unaffected protons would retain their peak sharpness and chemical shift values. This will only occur for interactions that do not lead to drastic alteration of chemical

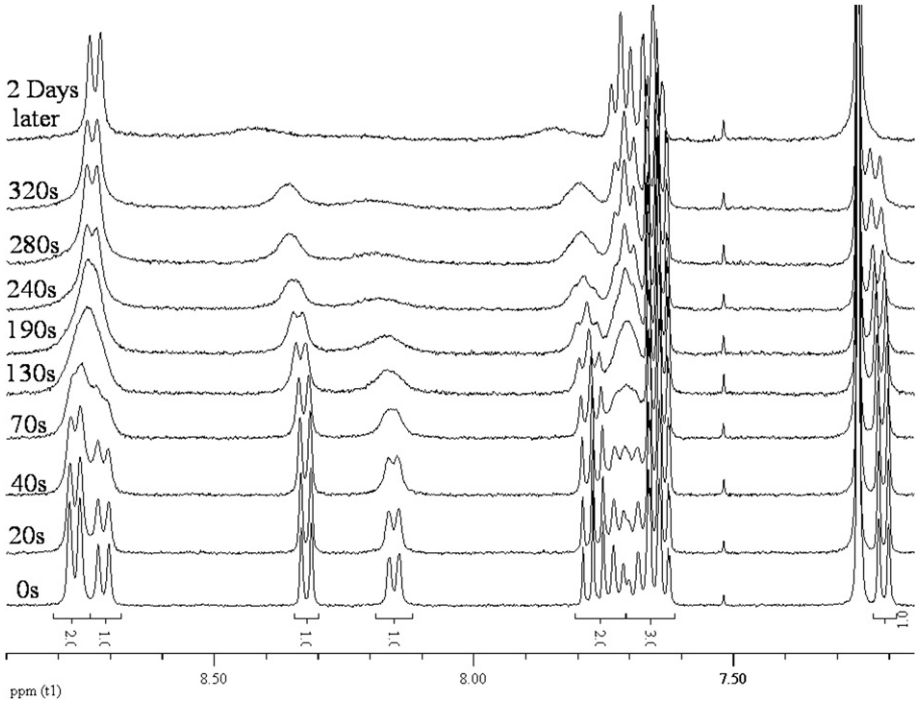

Fig. 9. Vertical stack of ^{1}H NMR of **3** in $CDCl_3$ at increasing exposure to UV radiation (300 nm).

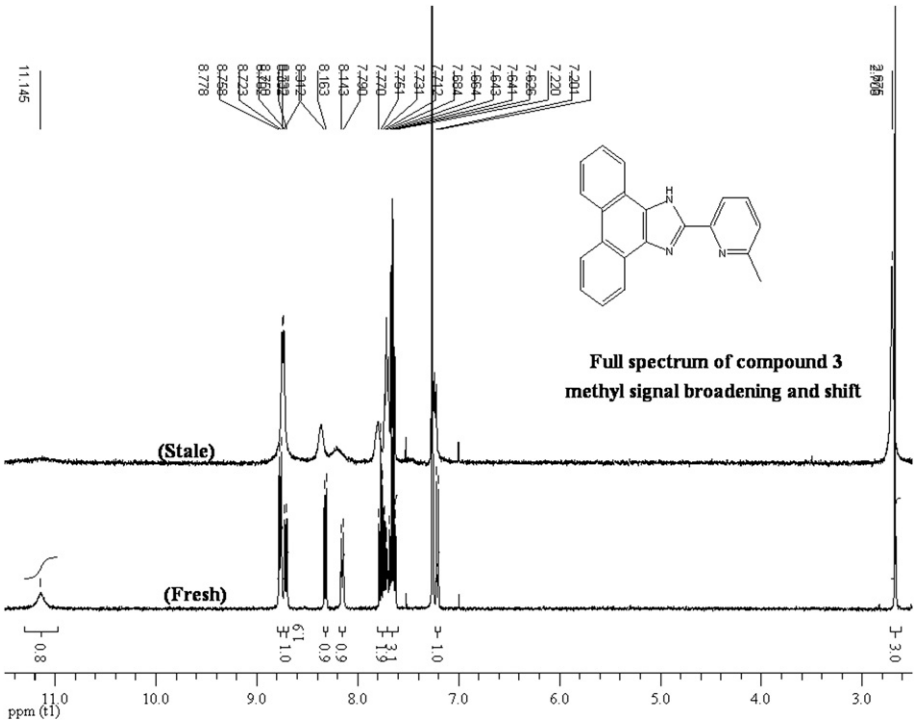

Fig. 10. Full spectrum of compound **3** showing methyl signal broadening and downfield shift.

structures. In efforts to further probe the nature of interactions that follows photo-excitation, proton chemical shifts were investigated for compounds **1**–**4** in *d*-$CHCl_3$ solutions at varying exposures times to 320 nm. The possibility of photo-stacking was thus supported in the cases of compounds **1** and **3** (Figs. 8 and 9 respectively). Only the imidazole analogues **1** and **3** gave dynamic changes since the time scale for reversal of photo-switching events observed in solutions of derivatives **2** and **4** were too short to observe changes in the regular ^{1}H NMR experiments.

It is also worthy of note that the active imidazole proton signals for **1** and **3** (δ_{N-H} = 11.14 ppm for **3**) also varnished during NMR studies, which indicates the importance of the N–H functionality in the proposed intermolecular interactions between molecules. We could observe that the pyridyl aromatic ring protons for ligand **1** were not affected in the process since only three protons were mainly downfield shifted as they became progressively broadened till they finally varnished. The coupling constants for the affected protons show they are neighbours. Other proton signals largely maintained their original chemical shift values and sharpness. Hence, the mode of interactions may involve the phenanthreneyl protons of compound **1** in a similar stacking manner to that observed in the X-ray structure of the phenanthreneyl ligand **11** (Fig. 3b). On the other hand, similar experiments on compound **3** revealed that five types of proton chemical shift environments underwent changes. This suggests that the whole length of the molecule is involved in intermolecular interaction (Fig. 9). This view is supported by methyl signal broadening and shift from 2.68 ppm to 2.71 ppm (Fig. 10). The reasoning is in line with the manner of interaction observed in solid state structure of the similarly methyl-substituted compound **9** (Fig. 2b). It is also important to mention that the ^{1}H NMR experiments conducted on samples already exposed to 320 nm irradiation and subsequently kept for days in the dark (wrapped in aluminium foil) still gave the same signals with varnished peaks for protons involved in intermolecular interaction. We therefore conclude that photo-induced fluorescent switching for compounds **1** and **3** is irreversible while being reversible for compounds **2** and **4**.

4. Conclusion

Twelve imidazole/oxazole based fluorophores, **1**–**12**, heterocycles were prepared and properly characterized. Structural characterizations were performed for **8**, **9** and **11**. On the basis of substituent factors, a comparative study of emission properties revealed that oxazole derivatives generally yielded better photoluminescence efficiencies compared to their imidazole analogues. Phenanthreneyl derivative **1**–**4** exhibited more promising characteristics in terms of emission efficiency and applicability for molecular signaling, etc. One interesting observation is that compound **3** exhibited a brilliant, green solid state photoluminescence, which may be suitable for organic lighting materials. Due to photo-induced intermolecular interactions in polar solvents, laser flashing of the oxazole analogues **2** and **4** produced reversible fluorescence switching between 400 nm and 550 nm of the visible spectrum, while the imidazole derivatives **1** and **3** showed irreversible fluorescence band changes in the same wavelength region. Pulse laser flash (355 nm) with 10 Hz irradiation and ^{1}H NMR experiments suggests that excimer species formed by **2** and **4** reverts to the initial molecular forms in short time scales. It is believed that compounds **2** and **4** are promising candidates for further investigations towards molecular sensing/signaling applications. Ligands **1** and **3** may find application in the areas of selective sensing of certain chemical species such as inorganic or organic ions, biochemicals, etc, that selectively hinders excimer formation or selectively unpacks photo-induced aggregation. Based on ^{1}H NMR studies, "offset face-to-face" stacking could not be ruled out.

Supplementary material

CCDC 761256, 761257 and 761258 contain the supplementary crystallographic data for compounds **8**, **9** and **11**. These data can be obtained free of charge on application to CCDC, 12 Union Road, Cambridge CB2 1EZ, UK (Fax: +44 01223 336033; e-mail: deposit@ccdc.cam.ac.uk).

Acknowledgement

The authors thank the National Natural Science Foundation of China for support of this research (Grant No. 20773149). A.O.E. is grateful to the Chinese Academy of Science (CAS), The Academy of Science for The Developing World (TWAS) for the Postgraduate Fellowships and Redeemer's University for granting study leave.

References

[1] De Silva AP, Gunaratne HQN, Gunnlaugsson T, Huxley ATM, McCoy CP, Rademacher JT, et al. Signaling recognition events with fluorescent sensors and switches. Chemical Reviews 1997;97:1515–66.
[2] MacDonald WA. Engineered films for display technologies. Journal of Material Chemistry 2004;14:4–10.
[3] Bettenhausen J, Greczmiel M, Jandke M, Strohriegl P. Oxadiazoles and phenylquinoxalines as electron transport materials. Synthetic Materials 1997; 91:223–8.
[4] Leevy WM, Gammon ST, Jiang H, Johnson JR, Maxwell DJ, Jackson EN, et al. Optical imaging of bacterial infection in living mice using a fluorescent near-infrared molecular probe. Journal of American Chemical Society 2006; 128:16476–7.
[5] Irie M, Fukaminato T, Sasaki T, Tamai N, Kawai T. A digital fluorescent molecular photoswitch. Nature 2002;420:759–60.
[6] Katoh A, Yoshida T, Ohkanda J. Synthesis of quinoxaline derivatives bearing the styryl and phenylethynyl groups and application to a fluorescence derivatization reagent. Heterocycles 2000;52:911–20.
[7] Liu S, Jiang P, Song GL, Liu R, Zhu HJ. Synthesis and optical properties of a series of thermally stable diphenylanthrazolines. Dyes and Pigments 2009; 81:218–23.
[8] Thirumurugan P, Muralidharan D, Perumal PT. The synthesis and photophysical studies of quinoxaline and pyridopyrazine derivatives. Dyes and Pigments 2009;81:245–53.
[9] Poteau X, Brown AI, Brown RG, Holmes C, Matthew D. Fluorescence switching in 4-amino-1,8-naphthalimides: "on–off–on" operation controlled by solvent and cations. Dyes and Pigments 2000;47:91–105.
[10] Imai Y, Shibata T, Makia S, Niwa H, Ohashi M, Hirano T. Fluorescence properties of phenolate anions of coelenteramide analogues: the light-emitter structure in aequorin bioluminescence. Journal of Photochemistry and Photobiology A: Chemistry 2001;146:95–107.
[11] Andresen M, Wahl MC, Stiel AC, Gräter F, Schäfer LV, Trowitzsch S, et al. Structure and mechanism of the reversible photoswitch of a fluorescent protein. Proceedings of the National Academy of Sciences (USA) 2005;102: 13070–4.
[12] Feng K, Hsu FH, Van DerVeer D, Bota K, Bu XR. Tuning fluorescence properties of imidazole derivatives with thiophene and thiazole. Journal of Photochemistry and Photobiology A: Chemistry 2004;165:223–8.
[13] Zhu M, Ahlberg PE, Zhao W, Jia L. A digital fluorescent molecular photoswitch. Nature 2002;420:759–60.
[14] Sun QJ, Fan BH, Tan ZA, Yang CH, Li FY, Yang Y. White light from polymer light-emitting diodes: utilization of fluorenone defects and exciplex. Applied Physics Letter 2006;88:163510–3.
[15] Du B, Liu R, Zhang Y, Yang W, Sun W, Sun M, et al. Novel chemosensory materials based on polyfluorenes with 2-(20-pyridyl)-benzimidazole and 5-methyl-3-(pyridin-2-yl)-1,2,4-triazole groups in the side chain. Polymer 2007;48:1245–54.
[16] Ying L, Zou J, Yang W, Zhang A, Wu Z, Zhao W, et al. Novel, blue light-emitting polyfluorenes containing a fluorinated quinoxaline unit. Dyes and Pigments 2009;82(3):251–7.
[17] Gong X, Moses D, Heeger AJ, Xiao S. White light electrophosphorescence from polyfluorene-based light-emitting diodes: utilization of fluorenone defects. Journal of Physical Chemistry B 2004;108:8601–5.
[18] Gong X, Ma W, Ostrowski JC, Bazan GC, Moses D, Heeger AJ. White electrophosphorescence from semiconducting polymer blends. Advanced Materials 2004;16:615–9.
[19] Tanaka I, Suzuki M, Tokito S. White light emission from polymer electrophosphorescent light-emitting devices doped with iridium complexes. Japanese Journal of Applied Physics, Part 1 2003;42:2737–40.
[20] Roxburgh CJ, Sammes PG, Abdullah A. Steric and substituent effects on the photoreversibility of novel indolospirobenzopyrans: acid deuterolysis, UV and ^{1}H NMR spectroscopy. Dyes and Pigments 2009;82:226–37.
[21] Park SY, Yoon JH, Hong CS, Souane R, Kim JS, Matthews SE, et al. A pyrenylppended triazole-based calix[4]arene as a fluorescent sensor for Cd^{2+} and Zn^{2+}. Journal of Organic Chemistry 2008;73:8212–8.
[22] Nagata Y, Chujo Y. Synthesis and luminescent properties of pyrenylvinylene-substituted tripylborane. Journal of Organometalic Chemistry 2009; 694:1723–6.
[23] Kondo M. Florescence spectra of 2-pyridylbenzimidazoles. A specific interaction of 2-(2-pyridyl)benzimidazole with ethanol. Bulletin of the Chemical Society of Japan 1978;51:3027–9.
[24] Bu L, Sawada T, Kuwahara Y, Shosenji H, Yoshida K. Crystallographic structure and solid-state fluorescence enhancement behavior of a 2-(9-anthryl)phenanthroimidazole-type clathrate host upon inclusion of amine molecules. Dyes and Pigments 2003;59:43–52.
[25] Mondal JA, Ramakrishna G, Singh AK, Ghosh HN, Mariappan M, Maiya BG, et al. Ultrafast intramolecular electronic energy-transfer dynamics in a bichromophoric molecule. Journal of Physical Chemistry A 2004;108:7843–52.
[26] Wang RY, Jia WL, Aziz H, Vamvounis G, Wang S, Hu NX, et al. 1-Methyl-2-(anthryl)-imidazo[4,5-f][1,10]-phenonthroline: a highly efficient electron-transport compound and a bright blue-light emitter for electroluminescent devices. Advanced Functional Materials 2005;15:1483–7.
[27] Xiao S, Yi T, Zhou Y, Zhao Q, Li F, Huang C. Multi-state molecular switches based on dithienylperfluorocyclopentene and imidazo[4,5-f][1,10]phenanthroline. Tetrahedron 2006;62:10072–8.
[28] Yan YX, Sun YH, Tian L, Fan HH, Wang HZ, Wang CK, et al. Synthesis, characterization and optical properties of a new heterocycle-based chromophores. Optical Materials 2007;30:423–6.
[29] Fang Z, Wang S, Zhao L, Dong B, Xu Z, Ren J, et al. A novel organic–inorganic hybrid fluorescent material as a selective chemosensor and adsorbent for Pb^{2+} ion. Materials Letters 2008;62:1514–7.
[30] Yang Y, Zeng MH, Zhao XH, Liang H. Supramolecular networks of hexanuclear cadmium(II): synthesis, crystal structure and emission property. Inorg. Chim. Acta 2009;362:3065–8.
[31] Sun M, Xin H, Wang KZ, Zhang YA, Jin LP, Huang CH. Bright and monochromic red light-emitting electroluminescence devices based on a new multifunctional europium ternary complex. Chemical Communications 2003;2003:702–3.
[32] Zhao YS, Peng A, Fu H, Ma Y, Yao J. Nanowire waveguides and ultraviolet lasers based on small organic molecules. Advanced Material 2008;20:1661–5.
[33] Eseola AO, Zhang M, Xiang JF, Zuo W, Li Y, Woods JAO, et al. Synthesis and characterization of nickel(II) complexes bearing 2-(imidazol-2-yl)pyridines or 2-(pyridin-2-yl) phenanthroimidazoles/oxazoles and their polymerization of norbornene. Inorg. Chim. Acta 2010;363:1970–8.
[34] Yamada M, Tanaka Y, Yoshimoo Y, Kuroda S, Shimao I. Ultrafast intramolecular electronic energy-transfer dynamics in a bichromophoric molecule. Bulletin of the Chemical Society of Japan 1992;65:1006.
[35] Dawson WR, Windsor MW. Fluorescence yields of aromatic compounds. Journal of Physical Chemistry 1968;72:3251–60.
[36] Hrdlovič P, Kollár J, Chmela S. Novel fluorescence probe based on pyrene and piperazine; spectral properties in solution and in polymer matrices. Journal of Photochemistry and Photobiology A: Chemistry 2004;163:289–96.
[37] Sheldrick GM. SHELXL-97, program for crystal structure analysis. Göttingen, Germany: University of Göttingen; 1997.
[38] Eseola AO, Li W, Gao R, Zhang M, Hao X, Liang T, et al. Synthesis, structures and fluorescent properties of 2-(1H-Imidazol-2-yl)phenols and their neutral Zn(II) complexes. Inorganic Chemistry 2009;48:9133–46.
[39] Zheng SL, Coppens P. Syntheses, structures, photoluminescence and theoretical studies of xanthone in crystalline resorcinarene-based inclusion complexes. Chemistry, A European Journal 2005;11:3583–90.